



1 The Role of Naphthalene and Its Derivatives in the
2 Formation of Secondary Organic Aerosols in the
3 Yangtze River Delta Region, China

4 *Fei Ye¹, Jingyi Li¹, Yaqin Gao², Hongli Wang², Jingyu An^{2,3}, Cheng Huang², Song Guo⁴, Keding*
5 *Lu⁴, Kangjia Gong¹, Haowen Zhang¹, Momei Qin¹, Jianlin Hu¹*

6 ¹ Jiangsu Key Laboratory of Atmospheric Environment Monitoring and Pollution Control,
7 Collaborative Innovation Center of Atmospheric Environment and Equipment Technology, School
8 of Environmental Science and Engineering, Nanjing University of Information Science &
9 Technology, Nanjing, 210044, China

10 ² State Environmental Protection Key Laboratory of the Formation and Prevention of Urban Air
11 Pollution Complex, Shanghai Academy of Environmental Sciences, Shanghai 200233, China

12 ³ Shanghai Key Laboratory of Atmospheric Particle Pollution and Prevention, Department of
13 Environmental Science and Engineering, Fudan University, Shanghai 200438, China

14 ⁴ State Key Joint Laboratory of Environmental Simulation and Pollution Control, College of
15 Environmental Sciences and Engineering, Peking University, Beijing, 100871, China

16 Correspondence to: Jingyi Li (jingyili@nuist.edu.cn), Jianlin Hu (jianlinhu@nuist.edu.cn)

17



18 **Abstract.** Naphthalene (Nap) and its derivatives, including 1-methylnaphthalene (1-MN) and 2-
19 methylnaphthalene (2-MN), serve as prominent intermediate volatile organic compounds (IVOCs)
20 contributing to the formation of secondary organic carbon (SOC). In this study, the Community
21 Multi-Scale Air Quality (CMAQ) model coupled with detailed emissions and reactions of these
22 compounds was utilized to examine their roles in the formation of SOC and other secondary
23 pollutants in the Yangtze River Delta (YRD) region during summer. Remarkably, significant
24 underestimations of Nap and MN concentrations (by 79% and 85%) were observed at the Taizhou
25 site. To better capture the temporal variations of Nap and MN, their emissions in the YRD region
26 were scaled up by a factor of 5 and 7, respectively, with constraints based on field measurements.
27 After adjusting their emissions, Nap concentrations reached 27 ppt in the YRD, accounting for 4.1%
28 and 9.1% (up to 13.7%) of total aromatics emissions and aromatic-derived SOC, respectively. 1-
29 MN and 2-MN were relatively low, with an average of 3 and 6 ppt in the YRD, and contributed
30 3.1% of aromatic-derived SOC. The influences of Nap and MN oxidation on ozone and radicals
31 might be trivial on a regional scale but were not negligible when considering daily fluctuations,
32 particularly in Shanghai and Suzhou. This study emphasizes the high SOC formation potentials of
33 Nap and MN, which may pose environmental risks and adverse health.

34 **1 Introduction**

35 Secondary organic aerosols (SOA) are formed from the condensation and multiphase
36 evolution of less volatile organic compounds (VOCs), which can be directly emitted or produced
37 from the oxidation of higher volatile organics in the atmosphere. SOA not only affects visibility
38 and human health but also has impacts on the climate directly by absorbing and reflecting solar
39 radiation and indirectly by affecting cloud formation (Chen et al., 2016; Zhang and Ying, 2012).
40 Semi-volatile and intermediate-volatile organic compounds (S/IVOCs) have been identified as the



41 key precursors of SOA (Robinson et al., 2007; Hu et al., 2022). IVOCs are categorized by small
42 polycyclic aromatic hydrocarbons (PAHs), intermediate-length alkanes (e.g. n-hexadecane), and
43 phenols (Pye and Seinfeld, 2010). PAHs are organic compounds containing multiple aromatic rings.
44 China was responsible for the highest annual PAH emissions at 114 Gg with a portion of 22% of
45 global total PAH emissions in 2004 (Zhang and Tao, 2009). Naphthalene (Nap) and
46 methylnaphthalene (MN), such as 1-methylnaphthalene (1-MN) and 2-methylnaphthalene (2-MN),
47 are the most abundant airborne PAHs (Chen et al., 2016; Fang et al., 2021), which are mainly
48 emitted from the combustion of fossil fuels, biomass burning, and industrial sectors (Fang et al.,
49 2021).

50 Chamber studies have identified the gas- and particle-phase products from Nap reacting with
51 hydroxyl radical (OH·) (Huang et al., 2019). Ring-retaining products (e.g., 1,4-naphthoquinone)
52 with lower volatilities are dominant under low nitrogen oxide (NO_x) conditions, and ring-opening
53 products (e.g., 2-formylcinnamaldehyde) with higher volatilities are dominant in the presence of
54 high NO_x. Chan et al. (2009) evaluated the SOA yields of Nap, 1-MN, 2-MN, and 1,2-dimethyl
55 naphthalene in chambers and applied these yields to estimate SOA formation from primary
56 emissions of diesel engines and wood burning. The SOA yields were 55–75% under low-NO_x
57 conditions at a total organic aerosol loading of 15 μg m⁻³, which was more efficient than high-NO_x
58 conditions (25–45%). In the photo-oxidation period of less than 12 h, these PAHs produced 3–5
59 times more SOA than light aromatic compounds and were responsible for up to 54% of total SOA
60 from the oxidation of diesel emissions. Huang et al. (2019) applied a tracer method and discovered
61 that 14.9% of SOA was owing to the oxidation of Nap and MN in the afternoon during the
62 wintertime haze in Beijing. Shakya and Griffin (2010) also reported 36–162 kg day⁻¹ of SOA
63 production from the mobile source emitted PAHs (including Nap, 1-MN, and 2-MN) in Houston



64 based on the yields from their study and that of Chan et al. (2009). Based on the yield from Shakya
65 and Griffin (2010), Liu et al. (2015) showed that Nap contributed 8–52% of the total SOA
66 originating from benzene, toluene, C2-benzene, C3-benzene, C4-benzene, and Nap in light-duty
67 gasoline vehicle exhausts. All these experimental findings demonstrate the significant role of Nap
68 and MN in SOA formation in the environment with anthropogenic influences dominated. However,
69 these results might not accurately reflect the actual atmospheric conditions due to the simplicity of
70 reaction conditions and the limited precursors involved in chamber studies (Ling et al., 2022).

71 Numerical models have been developed and utilized to assess the contribution of S/IVOCs to
72 SOA (Hayes et al., 2015; Pye and Seinfeld, 2010; An et al., 2023). Zhang and Ying (2011) showed
73 that PAHs emitted from anthropogenic sources could produce SOA mass as much as 10% of that
74 from the traditional light aromatics or around 4% of total anthropogenic SOA by using the
75 Community Multiscale Air Quality (CMAQ) model. However, the products from several explicit
76 PAH species (Nap, MN, dimethyl naphthalene, ethyl naphthalene, acenaphthylene, acenaphthene,
77 fluorene, phenanthrene, fluoranthene) were lumped rather than separated for their contributions to
78 SOA due to limited experimental data. Pye and Pouliot (2012) utilized the CMAQ model and
79 tracked 10% of peroxy radicals produced from the ARO2 (lumped aromatics in CMAQ) and OH·
80 reaction as for that of Nap without considering the emissions and the accurate OH· reactivity of
81 Nap. According to Cohan et al. (2013), the modeled SOA increased by roughly 1–10% when Nap
82 emissions from on-road gasoline and diesel vehicles were considered. Their simulations showed a
83 lower bound in the SOA production from Nap due to underestimations in the emission inventory
84 in the South Coast Air Basin of California. Majdi et al. (2019) found that Nap and MN contributed
85 2.4% to the total organic aerosol (OA) originating from wildfires over the Euro-Mediterranean



86 region during the summer of 2007 by using a 3D chemistry transport model (CTM). The
87 contributions of Nap and MN to SOA over a regional scale in China had not been quantified.

88 In this study, SOA formation from Nap, 1-MN, and 2-MN in the Yangtze River Delta (YRD)
89 region during the EXPLORE-YRD (EXPeriment on the eLucidation of the atmospheric Oxidation
90 capacity and aerosol foRmation, and their Effects in Yangtze River Delta) campaign period (May
91 20 – June 18, 2018) was investigated with an updated CMAQ model. Emission inventories of Nap,
92 1-MN, and 2-MN were estimated based on different sources and methods and validated against
93 observations. After that, the influences of Nap and MN on secondary organic carbon (SOC), ozone
94 (O_3), and radical concentrations in the locations with high concentrations and at the regional scale
95 were examined separately. The newly added SOA parameterizations for 1-MN and 2-MN were
96 fitted by both two-product and one-product methods to compare the differences. We find that Nap
97 and its derivatives, although accounting for a small fraction of emitted aromatics (5.1%),
98 contributed 12.1% of aromatic-derived SOC in the YRD.

99 **2 Methods**

100 **2.1 Modified SOA formation pathways of MN**

101 The CMAQ model version 5.2, coupled with the SAPRC07tic atmospheric chemical
102 mechanism and the AERO6i aerosol module, was updated to include the oxidation of 1-MN and
103 2-MN by $OH\cdot$ and the corresponding SOA formation pathways. In the original CMAQ model, Nap
104 reacts with $OH\cdot$ to form SOA under low- and high- NO_x conditions, which are represented by two
105 different counter species PAHHRXN and PAHNRXN, respectively (Fig. S1). Similar to Nap, 1-
106 MN, and 2-MN were treated explicitly as reacting with $OH\cdot$ and forming SOA counter species
107 under high NO_x (aMPAHNRXN and bMPAHNRXN) and low NO_x (aMPAHHRXN and
108 bMPAHHRXN), along with other products following Zhang and Ying (2012). These counter



109 species were used to calculate the production of SOA through gas-particle partitioning based on
110 yields (α_i) and partitioning coefficients ($K_{om,i}$, $\text{m}^3 \mu\text{g}^{-1}$) of condensable organic products derived
111 from chamber experiment data. The detailed descriptions of gas-particle partitioning to fit SOA
112 yield through one-product and two-product methods are depicted in the Supplement.

113 In gas-particle partitioning of the original CMAQ model, a two-product method (SV_PAH1
114 and SV_PAH2) was used to represent the SOA formation from Nap under high- NO_x conditions,
115 which are denoted as APAH1J and APAH2J respectively (Fig. S1a). Under low- NO_x conditions,
116 a one-product method was used to represent the SOA formation from Nap, denoted as APAH3J.
117 It was assumed that APAH3J (a yield of α_3) was non-volatile and resided in the particle phase.
118 Similar to Nap, a two-product method for the oxidation products of 1-MN was added under high-
119 NO_x conditions as shown in Fig. S1b, with the SOA species denoted as AaMPAH1J and
120 AaMPAH2J. A one-product method to characterize the oxidation products of 1-MN was also
121 applied to compare the difference caused by the fitting approach. As shown in Fig. S1c, the semi-
122 volatile organic product SV_aMPAH1' undergoes equilibrium partitioning to form SOA
123 (AaMPAH1J'). Under low- NO_x conditions, a non-volatile SOA product AaMPAH3J is formed by
124 the oxidation of 1-MN. The SOA pathways of 2-MN follow 1-MN, with the corresponding SOA
125 products of AbMPAH1J, AbMPAH2J, and AbMPAH3J, respectively. In addition, all semi-
126 volatile SOA products undergo condensed-phase oligomerization reactions at the same rate of
127 APAH1J and APAH2J and produce non-volatile oligomers (AOLGAJ) that belong to the
128 anthropogenic source. Other processes and parameters involved in the newly added SOA pathways
129 for 1-MN and 2-MN, such as the dry and wet deposition and the molecular weight of the oxidation
130 products were set to be the same as Nap due to limited experimental data. Details of all the
131 parameters, i.e., α_i , $K_{om,i}$, and $\Delta H_{vap,i}$ are summarized in Table S1.



132 **2.2 Model application**

133 The simulation domain, which covers Jiangsu, Zhejiang, Anhui, Shanghai, and neighboring
134 provinces, has a horizontal resolution of $4 \text{ km} \times 4 \text{ km}$ (238×268 grids) and a vertical structure of
135 18 layers as shown in Fig. S2. Details of the domain setup can be found in previous studies (Li et
136 al., 2021; Li et al., 2022). The meteorological field was predicted by the Weather Research and
137 Forecasting (WRF) model version 4.0 with the ECMWF Reanalysis v5.0 (ERA5) reanalysis data
138 as the inputs. More details about the WRF configuration were summarized by Wang et al. (2021).
139 A spin-up of two days was used to minimize the influence of initial conditions.

140 Biogenic emissions were generated from the Model for Emissions of Gases and Aerosols
141 from Nature (MEGAN) version 2.1 (Guenther et al., 2012). Open biomass burning emissions were
142 based on the Fire INventory from the National Center for Atmospheric Research (FINN)
143 (Wiedinmyer et al., 2011). Anthropogenic emissions were generated from the updated 2017
144 emission inventory for the YRD (Cheng et al., 2021) and the Multi-resolution Emission Inventory
145 for China (MEIC, <http://www.meicmodel.org>, last access: 1 June 2023) for the rest of the domain.
146 Currently, there is no available data to use in more localized sources in China. The detailed
147 emissions of 1-MN and 2-MN of different sources were calculated from the US EPA
148 (Environmental Protection Agency) repository of organic gas and PM speciation profiles of air
149 pollution sources (SPECIATEv5.2) and information reported by An et al. (2021) and Li et al.
150 (2014). See the Supplement for more details about the calculating process. There were two sets of
151 emission data consisting of different Nap and MN emissions in the YRD. The emis-orig used the
152 original Nap emissions from the 2017 YRD inventory and the calculated MN emissions. We show
153 later that Nap and MN were underestimated in emis-orig and required an adjustment in their
154 emissions to capture the observed concentrations. Therefore, the anthropogenic emissions of Nap



155 and MN in the YRD region from emis-orig were multiplied by 5 and 7, respectively, and
156 unchanged in other regions in the emis-adjust case. All the emission ratios applied in this study
157 are shown in Table S2. According to Fig. S3, Nap and MN emissions were mainly located in
158 Shanghai, southern Jiangsu, and parts of Zhejiang in the YRD region. After adjustments, the total
159 Nap and MN emission rate over the YRD region in emis-adjust (3.9 kg day^{-1}) was approximately
160 fourfold higher than that in emis-orig (0.9 kg day^{-1}). The total MN emission rate over the YRD
161 region in emis-adjust was 0.9 kg day^{-1} and was lower than that of Nap. For emis-adjust, the
162 dominant source of MN was residential-related (47.0%), followed by industry process (25.8%)
163 and on-road transport (20.8%). On-road transport contributed the most to Nap emissions in both
164 emis-orig (78.2%) and emis-adjust (87.5%). It should be noted that the source contributions of
165 Nap and MN may be influenced by the uncertainties in the source profiles.

166 Table S3 lists the scenarios conducted in this study. In case-1product-orig, the anthropogenic
167 emissions in the YRD used emis-orig with default Nap and added MN emissions, and the SOA
168 parameterization for MN was fitted by the one-product method. To assess the impacts of different
169 SOA parameterizations, the case-2products-orig shared the same setting with case-1product-orig
170 except that a two-product method for MN-generated SOA was employed. Both case-1product and
171 case-2products used emis-adjust as the emission inventory but different SOA parameterizations
172 for MN. In all, the contributions of Nap, 1-MN, and 2-MN to the aromatic SOC were estimated
173 based on different emission inventories and two SOA parameterization schemes. To evaluate the
174 effects of Nap, 1-MN, and 2-MN on O_3 , SOC, and radical concentrations, their emissions in case-
175 1product were set to zero and named base1.

176 **2.3 Observation data for model validation**



177 In May-June 2018, the EXPLORE-YRD field campaign was launched at a rural site in
178 Taizhou (32.558°N, 119.994°E) and simultaneously monitored VOCs (including Nap and MN),
179 O₃, NO_x, SOC, OH·, hydroperoxy radical (HO₂·), and other various pollutants, which provides a
180 good opportunity for model validation and understanding the evolution of air pollution in the YRD
181 (Wang et al., 2020; Huang et al., 2020; Yu et al., 2021; Gao et al., 2022). Details of the
182 measurement method and accuracy for each species refer to these references. The simulated
183 MDA8 O₃, fine particulate matter (PM_{2.5}), sulfur dioxide (SO₂), nitrogen dioxide (NO₂), and
184 carbon monoxide (CO) were also compared with the observations from the National Real-Time
185 Urban Air Quality Release Platform of the China Environmental Monitoring Center
186 (<http://106.37.208.233:20035/>, last access on May 17, 2023) in Suzhou, Nanjing, Hangzhou, Hefei,
187 and Shanghai cities as shown in Fig. S2. The statistical metrics including NMB, NME, and r were
188 calculated for several air pollution species. The model performance benchmarks followed the
189 recommendations by Emery et al. (2017) and are listed in Table S4. The meteorological parameters
190 predicted by WRF have been examined to be robust during the same episode by Wang et al. (2021).

191 **3 Results**

192 **3.1 Model validation**

193 Fig. 1 and Fig. S4 show the comparison of observed and simulated hourly variations of Nap,
194 MN, O₃, organic carbon (OC), and PM_{2.5} at the Taizhou site during the study period. As shown in
195 Fig. 1, in the original settings, the concentrations of Nap were largely underestimated in emis-orig
196 by 79% compared with the observations, with the value of NMB being -0.79. In contrast, emis-
197 adjust better represented the temporal variations of Nap (NMB=0.01, r=0.68) than emis-orig, with
198 the averaged concentration increased by 375% and more comparable to the observations. The
199 concentrations of MN simulated by emis-adjust (1.40E-2 ppb) were also comparable to the



200 observations ($1.50\text{E-}2$ ppb) and showed a good correlation with the observations ($r=0.59$). For
201 other species, the concentrations of OC and $\text{PM}_{2.5}$ were also improved in emis-adjust compared to
202 that of emis-orig, although they were underestimated in both scenarios. The NMB and NME of
203 $\text{PM}_{2.5}$ satisfied the benchmark recommended by Emery et al. (2017), while the NMB of the
204 maximum daily 8-hour average (MDA8) O_3 exceeded the benchmark. Table S5 shows that the
205 concentrations of NO_2 and nitric oxide (NO) were underestimated at the Taizhou site suggested by
206 the negative NMB values. The simulated OH radicals compared well with the observation while
207 the concentrations of $\text{HO}_2\cdot$ were underestimated at the Taizhou site (Fig. S5). The predicted
208 concentrations of MDA8 O_3 , $\text{PM}_{2.5}$, SO_2 , NO_2 , and CO were examined as shown in Table S4.
209 Overall, the model agreed well with observations in most of the cities except for a significant
210 underestimation of MAD8 O_3 in Shanghai. We chose the results from case-1product and case-
211 2products using emis-adjust as the emission data in the subsequent analysis.

212 **3.2 Influences of Nap and MN on SOC in Taizhou**

213 Figure 2 depicts the diurnal variations of emissions and concentrations of Nap, 1-MN, and 2-
214 MN, as well as the corresponding SOC products SOC-Nap, SOC-1MN, and SOC-2MN at the
215 Taizhou site in both case-1product and case-2products. The emissions of Nap, 1-MN, and 2-MN
216 exhibited a bimodal pattern. For Nap, the bimodal characteristics were the most pronounced,
217 accompanied by two peaks that occurred between 8:00~9:00 and 16:00~17:00, respectively. This
218 was likely attributed to the dominant source of Nap from transport as described in Sect. 2.2. Nap
219 and MN concentrations were relatively low during the daytime and peaked in the morning and at
220 night, which was caused by the fast photochemical removal and increased dilution during the
221 daytime, along with the facilitated accumulation due to low mixing heights at night (Cohan et al.,
222 2013; Huang et al., 2019). The concentrations of SOC generated by Nap, 1-MN, and 2-MN were



223 high during the daytime, especially from 10:00 to 15:00. This was attributed to the removal of Nap
224 and MN by OH radicals to form SOC. The potential removal by nighttime nitrate radicals (NO_3)
225 was negligible in this study, leading to a certain degree of declining trend for SOC formation at
226 night. Nap-derived SOC was the most abundant, followed by SOC from 2-MN (SOC-2MN) and
227 1-MN (SOC-1MN). This is attributed to the combined effects of the OH \cdot reactivity, SOA yields,
228 as well as abundances of the three compounds (Li et al., 2017; Yu et al., 2021). Apart from the
229 highest emissions of Nap, Nap is also more reactive with OH \cdot and has the highest SOA yield in
230 case-2products compared to the other two species. In case-1product, although the SOA yields of
231 MN are the highest, the OH \cdot reaction rate with Nap is faster than MN. The SOC generated by MN
232 in case-2products was lower than that in case-1product due to the lower SOA yield of MN applied
233 in case-2products as shown in Table S1.

234 Figure 3 shows the contributions of major aromatic species, i.e., Nap, 1-MN, 2-MN, 1,2,4-
235 trimethyl benzene (B124), xylene (MPO), benzene (BENZ), toluene (TOLU), aromatics with k_{OH}
236 (reaction rate constant with OH \cdot) $< 2 \times 10^4 \text{ ppm}^{-1} \text{ min}^{-1}$ (ARO1) and ARO2MN' (ARO2 excluding
237 Nap and MN) to the total emissions of aromatics and the aromatic-derived SOC in both case-
238 1product and case-2products at the Taizhou site. Among all the species, ARO2MN', MPO, and
239 B124 showed the largest fraction of emissions, accounting for 58.6%, followed by ARO1 and
240 TOLU (31.8%), and BENZ (6.3%). Nap and MN contributed the least to the total aromatic
241 emissions, with Nap to be the most abundant species. The daily average SOC produced from all
242 the aromatics was quite similar in case-1product and case-2products, which were 102.0 and 100.7
243 ng m^{-3} , respectively (Fig. S6). The contribution of ARO2MN', MPO, and B124 to the total
244 aromatic-derived SOC was the most significant, which was 45.2–45.8%. Nap showed a remarkable
245 contribution to SOC, accounting for 8.7–8.8%, although it only made up 2.6% of the total emitted



246 aromatics. 2-MN was also an important SOC precursor, contributing to 1.3–2.2% of the aromatic-
247 derived SOC. 1-MN was the least emitted aromatic compound, accounting for 0.2% of the total
248 aromatic emissions and less than 1.0% of the aromatic-derived SOC. All of Nap, 1-MN, and 2-
249 MN had the same trait of contributing much more to SOC than to SOC precursor emissions,
250 especially for Nap. The total contributions of MN and Nap to SOC were higher than that of BENZ,
251 even though their emissions were significantly lower than BENZ. Similar results were also found
252 in field campaigns conducted in Guangzhou (Fang et al., 2021) and Beijing (Huang et al., 2019)
253 where Nap and MN showed higher contributions. Compared to BENZ and other single-ring
254 aromatics, Nap and MN belong to IVOCs with lower saturation vapor pressure, which is more
255 likely to generate SOA through coagulation and absorption (Gao et al., 2021; Zhao et al., 2014).
256 Thus, their considerably higher SOA yields and reactivity with OH• lead to an important
257 contribution to SOA formation. In general, we found that 3.3% of aromatic emissions from Nap
258 and derivatives could contribute up to 11.7% SOC generated from aromatics at the Taizhou site.

259 **3.3 Regional distributions of Nap and MN and the influences on secondary pollutants**

260 In the YRD, the average contribution of Nap to aromatic emissions was 4.1% (Fig. S7), while
261 the Nap-derived SOC accounted for 9.0% and 9.1% of the total SOC generated by aromatics in
262 case-1product and case-2products, respectively. We found extremely high contributions of Nap-
263 derived SOC in areas with high Nap emissions (Fig. S8), reaching up to 13.7% in case-2products.
264 2-MN constituted 0.6% of the total aromatic emissions and contributed up to 3.8% of the aromatic-
265 derived SOC in case-1product. Among the three PAHs, 1-MN showed the lowest emissions (about
266 0.4% of the aromatic emissions) and the smallest regional average contribution to SOC (0.6–0.9%).
267 The SOC derived from MN in case-2products was approximately 38% lower than that in case-
268 1product across the entire YRD region (Fig. S8), while O₃ and the total SOC showed minor



269 differences in the two cases with different SOA parameterization of MN (Fig. S9). In general, the
270 concentrations of SOC produced by the three PAHs in case-1product were higher than those in
271 case-2products, which may minimize the discrepancy between the simulated and observed OC
272 given the existing underestimation of OC at least in Taizhou, as shown in Fig. 1 and Fig. S6.
273 Therefore, we opted for the results from case-1product in the subsequent analysis.

274 The accurate reproduction and quantitative constraints of Nap and MN are crucial for
275 understanding the atmospheric oxidation capacity in model simulations. The relative differences
276 between base1 and case-1product were calculated to evaluate the effects of Nap, 1-MN, and 2-MN
277 on O₃, SOC, and radical concentrations. As shown in Fig. 4a, the SOC concentrations over the
278 YRD region increased by approximately 1.0% on average, with the most significant increase
279 observed in areas with high emissions of Nap and MN, such as Shanghai and southern Jiangsu
280 Province, reaching up to 1.7%. The impact on O₃ was relatively limited, with a maximum increase
281 of 0.3%. Similar to SOC, the spatial distribution of O₃ variations was consistent with that of Nap
282 and MN emissions. When Nap and MN oxidation was considered in the model, HO₂· concentration
283 was enhanced across the domain by up to 1.6% (in Shanghai), due to the production of HO₂·
284 through the reaction of Nap and MN with OH·. However, the variations in OH· concentration
285 exhibited regional heterogeneity, with a maximum increase of 0.8% (in Shanghai) and a maximum
286 decrease of 0.3% (in Wenzhou). The areas with elevated OH· coincided with the locations
287 experiencing notable increases in O₃. As an OH· source in the troposphere, the photolysis of O₃
288 produces electronically excited O(¹D) atoms that react with water molecules to form fresh OH·
289 (Tan et al., 2019; Qin et al., 2022). Moreover, the areas with elevated OH· also exhibited a
290 significant increase in HO₂·. HO₂· can react with O₃ to produce OH·, thereby offsetting the OH·
291 consumption by Nap and MN oxidations (Zhu et al., 2020). In the areas with decreased OH·, the



292 increase of O_3 and $HO_2\cdot$ was not significant, resulting in fewer newly generated $OH\cdot$ to compensate
293 for the $OH\cdot$ consumption by Nap and MN.

294 To minimize the potential obfuscation of the true magnitude by the episode-average variation,
295 the hourly relative differences of SOC, O_3 , and radicals at the Shanghai and Suzhou sites, which
296 exhibit significant variations, are depicted in Fig. 4b and Fig. 4c, respectively. Overall, the
297 influences of Nap and MN varied daily. At the Shanghai site, the most pronounced effects of $OH\cdot$
298 and $HO_2\cdot$ were observed, with increases of up to 1.7% and 3.7%, respectively. At the Suzhou site,
299 the maximum daily variations of $OH\cdot$ and $HO_2\cdot$ (1.5% and 2.9%) were marginally lower than those
300 in Shanghai; whereas, the maximum daily variations of SOC and O_3 were elevated by 3.0% and
301 1.1% at the Suzhou site, respectively. Consequently, the influences of Nap and MN on SOC, O_3 ,
302 and the atmospheric oxidation capacity were substantial at the daily scale in those regions.

303 **4 Discussion**

304 Our results revealed that the contributions of Nap and MN to the total aromatic emissions
305 were minimal, which were 5.1% in the YRD and 3.3% at the Taizhou site. However, the SOC
306 produced by Nap and MN constituted 12.1% of the total aromatic-derived SOC in this region and
307 11.7% at the Taizhou site. Given the overestimation of other aromatic species in the current model
308 (Table S5), the contributions of Nap and MN to aromatic SOC might be underestimated. Yu et al.
309 (2021) demonstrated an augmented fraction of SOC derived from a yield method to that using the
310 EC tracer method after the inclusion of Nap and MN oxidation (from 25.3% to 39.5%) during the
311 same episode at the Taizhou site. That is to say, Nap and MN contributed 35.9% of the total SOC
312 estimated by using the SOA yield multiplied by the consumption of VOCs, which was higher than
313 the value (11.7%) in this study. Other field studies also found significant SOA formation from Nap
314 and MN among aromatics in the Pearl River Delta region (12.4%) (Fang et al., 2021) and in Beijing



315 during haze days ($10.2 \pm 1.3\%$) (Huang et al., 2019), with relatively smaller contributions to
316 emissions by 2% and 7%, respectively. This study highlights the crucial roles of Nap and MN,
317 which exhibit high SOA production potentials with trace amounts emitted into the atmosphere. In
318 addition, the average concentrations of Nap and MN in this study were 27 and 9 ppt during summer
319 over the YRD region (Fig. S8), respectively. Previous studies have confirmed that the
320 concentrations of Nap and MN exhibited a seasonal variation, with maxima in winter and minima
321 in summer, attributed to the increased heating and cooking activities in households during the cold
322 season (Tang et al., 2020; Huang et al., 2019; Fang et al., 2021). Consequently, the ambient
323 concentration of Nap and MN, along with the potential SOA production may be more severe in
324 winter. Cleaner fuel types and household cleaning products are recommended for vehicular and
325 domestic usage.

326 The urgent demand for enhancing the simulation and assessment of Nap and MN chemistry
327 is necessitated. Firstly, the characterization of Nap and MN from local sources and additional field
328 observations are indispensable to reduce the disparities between the modeled and observed Nap
329 and MN concentrations. Secondly, the SOA parameterizations of Nap and MN, including the
330 enthalpy of vaporization and SOA yields, are derived from limited chamber experiments and
331 require further validation. Previous studies have reported that the SOA yields obtained from
332 chamber studies were contingent on $\text{OH}\cdot$ exposure, NO_x levels, relative humidity, and seed
333 particles, which may not represent the actual atmospheric conditions (Yu et al., 2021; Ling et al.,
334 2022). Thirdly, chlorine radicals (Cl), NO_3 radicals, and O_3 also play an important role in the
335 atmospheric reactions of Nap and MN (Cohan et al., 2013; Matthieu et al., 2014; Riva et al., 2015;
336 Wang et al., 2005; Aleman, 2006), which were missing in the current study due to the lack of
337 parameterization. The formation of gas- and particle-phase products through reactions between



338 Cl atoms and Nap has been confirmed. For instance, chloronaphthalene and chloroacenaphthenone
339 have been identified as potential SOA markers for the Cl-initiated oxidation of Nap in the ambient
340 atmosphere (Riva et al., 2015). As important sources of Cl atoms, abundant nitryl chloride (ClNO₂)
341 and molecular chlorine (Cl₂) were attributed to sea salt, coal combustion, biomass burning (Le
342 Breton et al., 2018), and urban-originated transports (Li et al., 2021; Tham et al., 2013).
343 Consequently, the Cl-initiated SOA formation process may be pronounced in specific regions,
344 such as the marine boundary layer and industrial areas. Using the rate constant of Cl with Nap
345 $((4.22 \pm 0.46) \times 10^{-12})$ (Matthieu et al., 2014) and corresponding SOA yields (0.91 ± 0.05) (Riva et
346 al., 2015), which is approximately three times higher than those determined from OH-initiated
347 oxidation (Chan et al., 2009; Shakya and Griffin, 2010), we estimated the potential SOA formation
348 from the reaction of Nap and Cl atoms via a yield method (Huang et al., 2019; Yu et al., 2021).
349 Assuming a global average Cl concentration of 1×10^4 molecules cm⁻³ and a tropospheric lifetime
350 of 275 days as determined by Matthieu et al. (2014), SOA generated from Nap initiated by Cl
351 atoms is three times higher than that from the oxidation by OH· with a 12-h average daytime
352 concentration of 2×10^6 molecules cm⁻³ and a tropospheric lifetime of 6 hours. This suggests that
353 the omission of Cl-initiated chemistry in this study might lead to an underestimation of Nap-
354 derived SOA by approximately 75%. Given the underestimation of anthropogenic chlorine
355 emissions in China (Li et al., 2021; Choi et al., 2020), further studies are recommended to estimate
356 chlorine emissions with finer spatial resolution and the impacts on Nap SOA under
357 atmospherically realistic conditions. Lastly, a precise depiction of Nap and MN chemistry is
358 crucial for gaining a deeper understanding of the health implications of these noxious compounds.
359 The health risks associated with inhalation exposure to outdoor Nap and other PAHs have been
360 assessed by calculating the incremental lifetime cancer risk (ILCR) values in China and the United



361 States (Han et al., 2020; Zhang et al., 2016). Nonetheless, there has been no systematic evaluation
362 of the health risks resulting from exposure to PAH-derived SOA and by-products, despite previous
363 studies verifying the toxicological impacts (e.g. oxidation potential, OP) of Nap-derived SOA
364 (Lima de Albuquerque et al., 2021; Wang et al., 2018; Tuet et al., 2017a; Tuet et al., 2017b). More
365 precise measurements of the OP of the different individual SOA are needed in order to evaluate
366 the overall oxidative potentials of ambient SOA using individual intrinsic OP of different types of
367 SOA in conjunction with SOA loadings in models. Future studies are needed to develop rational
368 parameterization schemes for assessing the health risks associated with Nap- and MN-derived
369 SOA.

370 **5 Conclusions**

371 In this study, we investigated the impacts of Nap, 1-MN, and 2-MN oxidation on the
372 formation of SOC, O₃, and radicals from May 20 to June 18, 2018, in the YRD using a revised
373 CMAQ model and explicit emission inventories. The simulating results of case-Iproduct using the
374 adjusted emissions (emis-adjust) and a one-product method to fit MN yields best reproduced the
375 evolution of Nap (NMB=0.01) and MN (NMB=-0.07) when compared with the default case
376 (NMB=-0.79 for Nap, NMB=-0.85 for MN). The primary sources of Nap and MN were
377 transportation and residential-related and thus led to a bimodal pattern for their emissions. Whereas
378 the Nap and MN concentrations were relatively low during the daytime and peaked in the morning,
379 the generated SOC peaked in the daytime affected by the photochemistry and the evolution of the
380 boundary layer. All of Nap, 1-MN, and 2-MN had the same trait of contributing much more to
381 SOC than to SOC precursor emissions, especially for Nap. In general, we found that 3.3% of
382 aromatic emissions from Nap and derivatives could contribute up to 11.7% SOC generated from
383 aromatics at the Taizhou site. Nap concentrations reached 27 ppt in the YRD, accounting for 4.1%



384 and 9.1% (up to 13.7%) of total aromatics emissions and aromatic-derived SOC, respectively. 1-
385 MN and 2-MN were relatively low, with an average of 3 and 6 ppt in the YRD, and contributed
386 3.1% of aromatic-derived SOC. At the regional scale, the impacts of Nap and MN oxidation on O₃
387 and radical concentrations were limited. However, substantial increases still occurred in areas with
388 high Nap and MN emissions and cannot be disregarded. The high SOA formation potential of Nap
389 and MN and its impact on secondary pollutants proved in this study implied the significance of
390 such IVOCs except for traditional VOCs when implementing air pollution control policies, energy
391 use strategies, and health risks evaluation.

392

393 **Code and data availability**

394 The codes used for all the analyses are available on reasonable request to the corresponding author.
395 All data used in this research are freely available and may be downloaded from the links and cited
396 references given in the methods section.

397 **Author contributions**

398 F.Y., J.L., and J.H. designed the research and conducted the simulations, Y.G., H.W., S.G., and
399 K.L. collected the observed data. J.A. and C.H. provided emission data. F.Y., J.L., J.H., and M.Q.
400 analyzed the data, all authors discussed the results. F.Y. prepared the manuscript and all authors
401 helped improve the manuscript.

402 **Competing interests**

403 The authors declare no competing interests.

404 **Disclaimer**



405 Publisher's note: Copernicus Publications remains neutral with regard to jurisdictional claims
406 made in the text, published maps, institutional affiliations, or any other geographical representation
407 in this paper. While Copernicus Publications makes every effort to include appropriate place
408 names, the final responsibility lies with the authors.

409 **Acknowledgements**

410 This work was financially supported by the National Key R&D Program of China
411 (2022YFE0136200) and the National Natural Science Foundation of China (No. 42077199).

412 **References**

- 413 Aleman, G.: The kinetics and mechanisms of chlorine atom reactions with alkylbenzenes and
414 alkylnaphthalenes, California State University, Fullerton., 2006.
- 415 An, J., Huang, C., Huang, D., Qin, M., Liu, H., Yan, R., Qiao, L., Zhou, M., Li, Y., Zhu, S., Wang,
416 Q., and Wang, H.: Sources of organic aerosols in eastern China: a modeling study with high-
417 resolution intermediate-volatility and semivolatile organic compound emissions, *Atmos. Chem.*
418 *Phys.*, 23, 323-344, 10.5194/acp-23-323-2023, 2023.
- 419 An, J., Huang, Y., Huang, C., Wang, X., Yan, R., Wang, Q., Wang, H., Jing, S. a., Zhang, Y., Liu,
420 Y., Chen, Y., Xu, C., Qiao, L., Zhou, M., Zhu, S., Hu, Q., Lu, J., and Chen, C.: Emission inventory
421 of air pollutants and chemical speciation for specific anthropogenic sources based on local
422 measurements in the Yangtze River Delta region, China, *Atmospheric Chemistry and Physics*, 21,
423 2003-2025, 10.5194/acp-21-2003-2021, 2021.
- 424 Chan, A. W. H., Kautzman, K. E., Chhabra, P. S., Surratt, J. D., Chan, M. N., Crounse, J. D., Kürten,
425 A., Wennberg, P. O., Flagan, R. C., and Seinfeld, J. H.: Secondary organic aerosol formation from
426 photooxidation of naphthalene and alkylnaphthalenes: implications for oxidation of intermediate
427 volatility organic compounds (IVOCs), *Atmos. Chem. Phys.*, 9, 3049-3060, 10.5194/acp-9-3049-
428 2009, 2009.
- 429 Chen, C.-L., Kacarab, M., Tang, P., and Cocker, D. R.: SOA formation from naphthalene, 1-
430 methylnaphthalene, and 2-methylnaphthalene photooxidation, *Atmospheric Environment*, 131,
431 424-433, 10.1016/j.atmosenv.2016.02.007, 2016.
- 432 Cheng, Y., Yu, Q.-q., Liu, J.-m., Du, Z.-Y., Liang, L.-l., Geng, G.-n., Zheng, B., Ma, W.-l., Qi, H.,
433 Zhang, Q., and He, K.-b.: Strong biomass burning contribution to ambient aerosol during heating
434 season in a megacity in Northeast China: Effectiveness of agricultural fire bans?, *Science of The*
435 *Total Environment*, 754, 10.1016/j.scitotenv.2020.142144, 2021.
- 436 Choi, M. S., Qiu, X., Zhang, J., Wang, S., Li, X., Sun, Y., Chen, J., and Ying, Q.: Study of
437 Secondary Organic Aerosol Formation from Chlorine Radical-Initiated Oxidation of Volatile
438 Organic Compounds in a Polluted Atmosphere Using a 3D Chemical Transport Model,
439 *Environmental Science & Technology*, 54, 13409-13418, 10.1021/acs.est.0c02958, 2020.
- 440 Cohan, A., Eiguren-Fernandez, A., Miguel, A. H., and Dabdub, D.: Secondary organic aerosol
441 formation from naphthalene roadway emissions in the South Coast Air Basin of California,
442 *International Journal of Environment and Pollution*, 52, 206-224, 10.1504/IJEP.2013.058461,



- 443 2013.
- 444 Emery, C., Liu, Z., Russell, A. G., Odman, M. T., Yarwood, G., and Kumar, N.: Recommendations
445 on statistics and benchmarks to assess photochemical model performance, *J Air Waste Manag*
446 *Assoc*, 67, 582-598, 10.1080/10962247.2016.1265027, 2017.
- 447 Fang, H., Luo, S., Huang, X., Fu, X., Xiao, S., Zeng, J., Wang, J., Zhang, Y., and Wang, X.:
448 Ambient naphthalene and methylnaphthalenes observed at an urban site in the Pearl River Delta
449 region: Sources and contributions to secondary organic aerosol, *Atmospheric Environment*, 252,
450 10.1016/j.atmosenv.2021.118295, 2021.
- 451 Gao, Y., Li, M., Wan, X., Zhao, X., Wu, Y., Liu, X., and Li, X.: Important contributions of alkenes
452 and aromatics to VOCs emissions, chemistry and secondary pollutants formation at an industrial
453 site of central eastern China, *Atmospheric Environment*, 244, 10.1016/j.atmosenv.2020.117927,
454 2021.
- 455 Gao, Y., Wang, H., Liu, Y., Zhang, X., Jing, S., Peng, Y., Huang, D., Li, X., Chen, S., Lou, S., Li,
456 Y., and Huang, C.: Unexpected High Contribution of Residential Biomass Burning to Non-
457 Methane Organic Gases (NMOGs) in the Yangtze River Delta Region of China, *Journal of*
458 *Geophysical Research: Atmospheres*, 127, 10.1029/2021jd035050, 2022.
- 459 Guenther, A. B., Jiang, X., Heald, C. L., Sakulyanontvittaya, T., Duhl, T., Emmons, L. K., and
460 Wang, X. J. G. M. D.: The Model of Emissions of Gases and Aerosols from Nature version 2.1
461 (MEGAN2.1): an extended and updated framework for modeling biogenic emissions, 5, 1471-
462 1492, 2012.
- 463 Han, F., Guo, H., Hu, J., Zhang, J., Ying, Q., and Zhang, H.: Sources and health risks of ambient
464 polycyclic aromatic hydrocarbons in China, *Sci Total Environ*, 698, 134229,
465 10.1016/j.scitotenv.2019.134229, 2020.
- 466 Hayes, P. L., Carlton, A. G., Baker, K. R., Ahmadov, R., Washenfelder, R. A., Alvarez, S.,
467 Rappenglück, B., Gilman, J. B., Kuster, W. C., de Gouw, J. A., Zotter, P., Prévôt, A. S. H., Szidat,
468 S., Kleindienst, T. E., Offenberg, J. H., Ma, P. K., and Jimenez, J. L.: Modeling the formation and
469 aging of secondary organic aerosols in Los Angeles during CalNex 2010, *Atmospheric Chemistry*
470 *and Physics*, 15, 5773-5801, 10.5194/acp-15-5773-2015, 2015.
- 471 Hu, W., Zhou, H., Chen, W., Ye, Y., Pan, T., Wang, Y., Song, W., Zhang, H., Deng, W., Zhu, M.,
472 Wang, C., Wu, C., Ye, C., Wang, Z., Yuan, B., Huang, S., Shao, M., Peng, Z., Day, D. A.,
473 Campuzano-Jost, P., Lambe, A. T., Worsnop, D. R., Jimenez, J. L., and Wang, X.: Oxidation Flow
474 Reactor Results in a Chinese Megacity Emphasize the Important Contribution of S/IVOCs to
475 Ambient SOA Formation, *Environ Sci Technol*, 56, 6880-6893, 10.1021/acs.est.1c03155, 2022.
- 476 Huang, D. D., Kong, L., Gao, J., Lou, S., Qiao, L., Zhou, M., Ma, Y., Zhu, S., Wang, H., Chen, S.,
477 Zeng, L., and Huang, C.: Insights into the formation and properties of secondary organic aerosol
478 at a background site in Yangtze River Delta region of China: Aqueous-phase processing vs.
479 photochemical oxidation, *Atmospheric Environment*, 239, 117716,
480 <https://doi.org/10.1016/j.atmosenv.2020.117716>, 2020.
- 481 Huang, G., Liu, Y., Shao, M., Li, Y., Chen, Q., Zheng, Y., Wu, Z., Liu, Y., Wu, Y., Hu, M., Li, X.,
482 Lu, S., Wang, C., Liu, J., Zheng, M., and Zhu, T.: Potentially Important Contribution of Gas-Phase
483 Oxidation of Naphthalene and Methylnaphthalene to Secondary Organic Aerosol during Haze
484 Events in Beijing, *Environ Sci Technol*, 53, 1235-1244, 10.1021/acs.est.8b04523, 2019.
- 485 Le Breton, M., Hallquist, Å. M., Pathak, R. K., Simpson, D., Wang, Y., Johansson, J., Zheng, J.,
486 Yang, Y., Shang, D., Wang, H., Liu, Q., Chan, C., Wang, T., Bannan, T. J., Priestley, M., Percival,
487 C. J., Shallcross, D. E., Lu, K., Guo, S., Hu, M., and Hallquist, M.: Chlorine oxidation of VOCs at
488 a semi-rural site in Beijing: significant chlorine liberation from ClNO₂ and subsequent gas- and



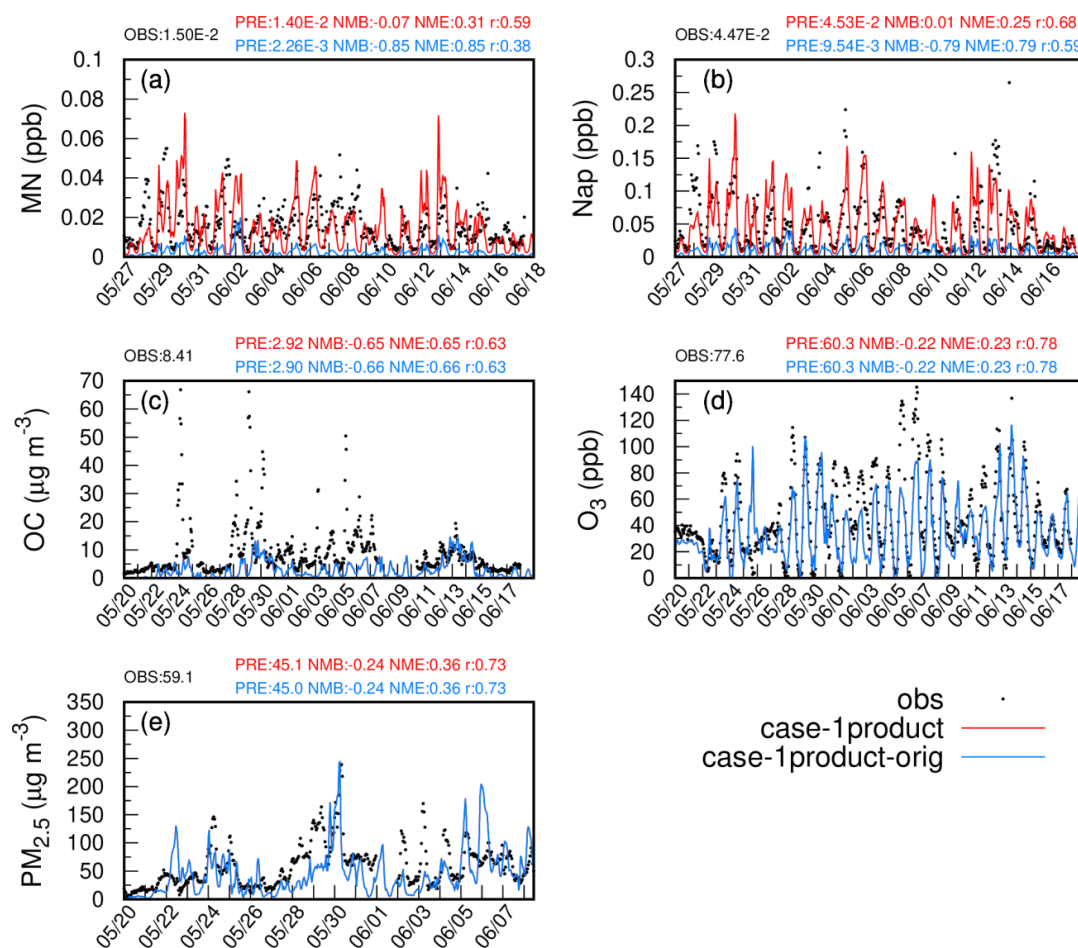
- 489 particle-phase Cl–VOC production, *Atmos. Chem. Phys.*, 18, 13013–13030, 10.5194/acp-18-
490 13013–2018, 2018.
- 491 Li, J., Zhang, M., Wu, F., Sun, Y., and Tang, G.: Assessment of the impacts of aromatic VOC
492 emissions and yields of SOA on SOA concentrations with the air quality model RAMS-CMAQ,
493 *Atmospheric Environment*, 158, 105–115, 10.1016/j.atmosenv.2017.03.035, 2017.
- 494 Li, J., Zhang, N., Wang, P., Choi, M., Ying, Q., Guo, S., Lu, K., Qiu, X., Wang, S., Hu, M., Zhang,
495 Y., and Hu, J.: Impacts of chlorine chemistry and anthropogenic emissions on secondary pollutants
496 in the Yangtze river delta region, *Environmental Pollution*, 287, 117624,
497 <https://doi.org/10.1016/j.envpol.2021.117624>, 2021.
- 498 Li, L., Xie, F., Li, J., Gong, K., Xie, X., Qin, Y., Qin, M., and Hu, J.: Diagnostic analysis of regional
499 ozone pollution in Yangtze River Delta, China: A case study in summer 2020, *Sci Total Environ*,
500 812, 151511, 10.1016/j.scitotenv.2021.151511, 2022.
- 501 Li, M., Zhang, Q., Streets, D. G., He, K. B., Cheng, Y. F., Emmons, L. K., Huo, H., Kang, S. C.,
502 Lu, Z., Shao, M., Su, H., Yu, X., and Zhang, Y.: Mapping Asian anthropogenic emissions of non-
503 methane volatile organic compounds to multiple chemical mechanisms, *Atmos. Chem. Phys.*, 14,
504 5617–5638, 10.5194/acp-14-5617-2014, 2014.
- 505 Lima de Albuquerque, Y., Berger, E., Tomaz, S., George, C., and Geloën, A.: Evaluation of the
506 Toxicity on Lung Cells of By-Products Present in Naphthalene Secondary Organic Aerosols, *Life*
507 (Basel), 11, 10.3390/life11040319, 2021.
- 508 Ling, Z., Wu, L., Wang, Y., Shao, M., Wang, X., and Huang, W.: Roles of semivolatile and
509 intermediate-volatility organic compounds in secondary organic aerosol formation and its
510 implication: A review, *J Environ Sci (China)*, 114, 259–285, 10.1016/j.jes.2021.08.055, 2022.
- 511 Liu, T., Wang, X., Deng, W., Hu, Q., Ding, X., Zhang, Y., He, Q., Zhang, Z., Lü, S., Bi, X., Chen,
512 J., and Yu, J.: Secondary organic aerosol formation from photochemical aging of light-duty
513 gasoline vehicle exhausts in a smog chamber, *Atmospheric Chemistry and Physics*, 15, 9049–9062,
514 10.5194/acp-15-9049-2015, 2015.
- 515 Majdi, M., Sartelet, K., Lanzafame, G. M., Couvidat, F., Kim, Y., Chrit, M., and Turquety, S.:
516 Precursors and formation of secondary organic aerosols from wildfires in the Euro-Mediterranean
517 region, *Atmospheric Chemistry and Physics*, 19, 5543–5569, 10.5194/acp-19-5543-2019, 2019.
- 518 Matthieu, Riva, Robert, M., Healy, Pierre-Marie, Flaud, Emilie, Perraudin, and A, J. J. J. o. P. C.:
519 Kinetics of the Gas-Phase Reactions of Chlorine Atoms with Naphthalene, Acenaphthene, and
520 Acenaphthylene, 2014.
- 521 Pye, H. O. and Pouliot, G. A.: Modeling the role of alkanes, polycyclic aromatic hydrocarbons,
522 and their oligomers in secondary organic aerosol formation, *Environ Sci Technol*, 46, 6041–6047,
523 10.1021/es300409w, 2012.
- 524 Pye, H. O. T. and Seinfeld, J. H.: A global perspective on aerosol from low-volatility organic
525 compounds, *Atmospheric Chemistry and Physics*, 10, 4377–4401, 10.5194/acp-10-4377-2010,
526 2010.
- 527 Qin, M., Hu, A., Mao, J., Li, X., Sheng, L., Sun, J., Li, J., Wang, X., Zhang, Y., and Hu, J.: PM(2.5)
528 and O(3) relationships affected by the atmospheric oxidizing capacity in the Yangtze River Delta,
529 China, *Sci Total Environ*, 810, 152268, 10.1016/j.scitotenv.2021.152268, 2022.
- 530 Riva, M., Healy, R. M., Flaud, P. M., Perraudin, E., Wenger, J. C., and Villenave, E. J. J. o. P. C.
531 A.: Gas- and Particle-Phase Products from the Chlorine-Initiated Oxidation of Polycyclic Aromatic
532 Hydrocarbons, 11170–11181, 2015.
- 533 Robinson, A. L., Donahue, N. M., Shrivastava, M. K., Weitkamp, E. A., Sage, A. M., Grieshop, A.
534 P., Lane, T. E., Pierce, J. R., and Pandis, S. N.: Rethinking organic aerosols: semivolatile emissions



- 535 and photochemical aging, *Science*, 315, 1259-1262, 10.1126/science.1133061, 2007.
- 536 Shakya, K. M. and Griffin, R. J.: Secondary Organic Aerosol from Photooxidation of Polycyclic
537 Aromatic Hydrocarbons, *Environmental Science & Technology*, 44, 8134-8139,
538 10.1021/es1019417, 2010.
- 539 Tan, Z., Lu, K., Hofzumahaus, A., Fuchs, H., Bohn, B., Holland, F., Liu, Y., Rohrer, F., Shao, M.,
540 Sun, K., Wu, Y., Zeng, L., Zhang, Y., Zou, Q., Kiendler-Scharr, A., Wahner, A., and Zhang, Y.:
541 Experimental budgets of OH, HO₂, and RO₂
542 radicals and implications for ozone formation in the Pearl River Delta in China 2014, *Atmospheric
543 Chemistry and Physics*, 19, 7129-7150, 10.5194/acp-19-7129-2019, 2019.
- 544 Tang, T., Cheng, Z., Xu, B., Zhang, B., Zhu, S., Cheng, H., Li, J., Chen, Y., and Zhang, G.: Triple
545 Isotopes ($\delta^{13}\text{C}$, $\delta^2\text{H}$, and $\Delta^{14}\text{C}$) Compositions and Source Apportionment of Atmospheric
546 Naphthalene: A Key Surrogate of Intermediate-Volatility Organic Compounds (IVOCs),
547 *Environmental Science & Technology*, 54, 5409-5418, 10.1021/acs.est.0c00075, 2020.
- 548 Tham, Y. J., Yan, C., Xue, L., Zha, Q., Wang, X., and Wang, T. J. C. S. B.: Presence of high nitryl
549 chloride in Asian coastal environment and its impact on atmospheric photochemistry, 2013.
- 550 Tuet, W. Y., Chen, Y., Fok, S., Gao, D., Weber, R. J., Champion, J. A., and Ng, N. L.: Chemical
551 and cellular oxidant production induced by naphthalene secondary organic aerosol (SOA): effect
552 of redox-active metals and photochemical aging, *Sci Rep*, 7, 15157, 10.1038/s41598-017-15071-
553 8, 2017a.
- 554 Tuet, W. Y., Chen, Y., Xu, L., Fok, S., Gao, D., Weber, R. J., and Ng, N. L.: Chemical oxidative
555 potential of secondary organic aerosol (SOA) generated from the photooxidation of biogenic and
556 anthropogenic volatile organic compounds, *Atmospheric Chemistry and Physics*, 17, 839-853,
557 10.5194/acp-17-839-2017, 2017b.
- 558 Wang, H., Chen, X., Lu, K., Hu, R., Li, Z., Wang, H., Ma, X., Yang, X., Chen, S., Dong, H., Liu,
559 Y., Fang, X., Zeng, L., Hu, M., and Zhang, Y.: NO₃ and N₂O₅ chemistry at a suburban site during
560 the EXPLORE-YRD campaign in 2018, *Atmospheric Environment*, 224,
561 10.1016/j.atmosenv.2019.117180, 2020.
- 562 Wang, L., Arey, J., and Atkinson, R.: Reactions of Chlorine Atoms with a Series of Aromatic
563 Hydrocarbons, *Environmental Science & Technology*, 39, 5302-5310, 10.1021/es0479437, 2005.
- 564 Wang, S., Ye, J., Soong, R., Wu, B., Yu, L., Simpson, A. J., and Chan, A. W. H.: Relationship
565 between chemical composition and oxidative potential of secondary organic aerosol from
566 polycyclic aromatic hydrocarbons, *Atmospheric Chemistry and Physics*, 18, 3987-4003,
567 10.5194/acp-18-3987-2018, 2018.
- 568 Wang, X., Li, L., Gong, K., Mao, J., Hu, J., Li, J., Liu, Z., Liao, H., Qiu, W., Yu, Y., Dong, H., Guo,
569 S., Hu, M., Zeng, L., and Zhang, Y.: Modelling air quality during the EXPLORE-YRD campaign
570 – Part I. Model performance evaluation and impacts of meteorological inputs and grid resolutions,
571 *Atmospheric Environment*, 246, 10.1016/j.atmosenv.2020.118131, 2021.
- 572 Wiedinmyer, C., Akagi, S. K., Yokelson, R. J., Emmons, L. K., Al-Saadi, J. A., Orlando, J. J., and
573 Soja, A. J.: The Fire INventory from NCAR (FINN): a high resolution global model to estimate
574 the emissions from open burning, *Geosci. Model Dev.*, 4, 625-641, 10.5194/gmd-4-625-2011,
575 2011.
- 576 Yu, Y., Wang, H., Wang, T., Song, K., Tan, T., Wan, Z., Gao, Y., Dong, H., Chen, S., Zeng, L., Hu,
577 M., Wang, H., Lou, S., Zhu, W., and Guo, S.: Elucidating the importance of semi-volatile organic
578 compounds to secondary organic aerosol formation at a regional site during the EXPLORE-YRD
579 campaign, *Atmospheric Environment*, 246, 10.1016/j.atmosenv.2020.118043, 2021.
- 580 Zhang, H. and Ying, Q.: Secondary organic aerosol formation and source apportionment in

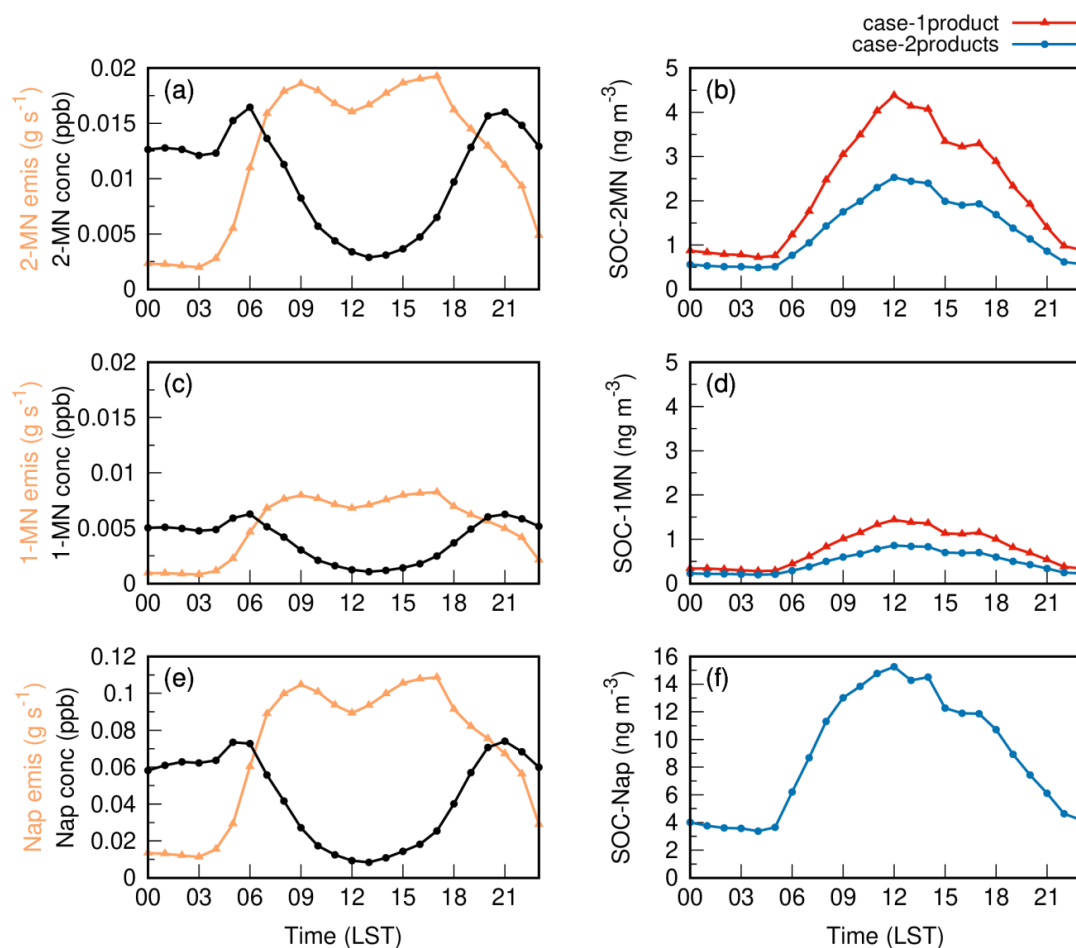


- 581 Southeast Texas, Atmospheric Environment, 45, 3217-3227, 10.1016/j.atmosenv.2011.03.046,
582 2011.
- 583 Zhang, H. and Ying, Q.: Secondary organic aerosol from polycyclic aromatic hydrocarbons in
584 Southeast Texas, Atmospheric environment, 55, 279-287, 2012.
- 585 Zhang, J., Wang, P., Li, J., Mendola, P., Sherman, S., and Ying, Q.: Estimating population exposure
586 to ambient polycyclic aromatic hydrocarbon in the United States - Part II: Source apportionment
587 and cancer risk assessment, Environ Int, 97, 163-170, 10.1016/j.envint.2016.08.024, 2016.
- 588 Zhang, Y. and Tao, S.: Global atmospheric emission inventory of polycyclic aromatic
589 hydrocarbons (PAHs) for 2004, Atmospheric Environment, 43, 812-819,
590 10.1016/j.atmosenv.2008.10.050, 2009.
- 591 Zhao, Y., Hennigan, C. J., May, A. A., Tkacik, D. S., de Gouw, J. A., Gilman, J. B., Kuster, W. C.,
592 Borbon, A., and Robinson, A. L.: Intermediate-Volatility Organic Compounds: A Large Source of
593 Secondary Organic Aerosol, Environmental Science & Technology, 48, 13743-13750,
594 10.1021/es5035188, 2014.
- 595 Zhu, J., Wang, S., Wang, H., Jing, S., Lou, S., Saiz-Lopez, A., and Zhou, B.: Observationally
596 constrained modeling of atmospheric oxidation capacity and photochemical reactivity in Shanghai,
597 China, Atmospheric Chemistry and Physics, 20, 1217-1232, 10.5194/acp-20-1217-2020, 2020.



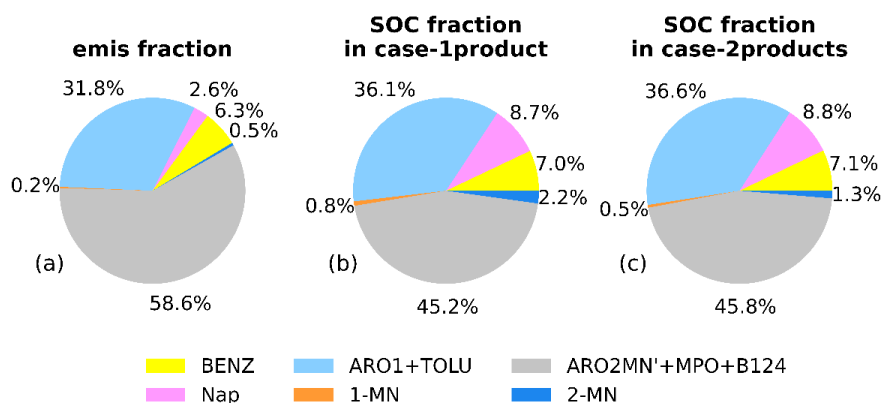
598

599 **Figure 1.** Observed and simulated hourly concentrations of MN, Nap, OC, PM_{2.5}, and O₃ based
 600 on emis-adjust (red) and emis-orig (blue) at the Taizhou site. Model performances of daily MN,
 601 Nap, OC, PM_{2.5}, and MDA8 O₃ are shown in blue for case-1product-orig and red for case-1product.
 602 OBS and PRE represent averaged concentrations of observations and predictions, respectively.



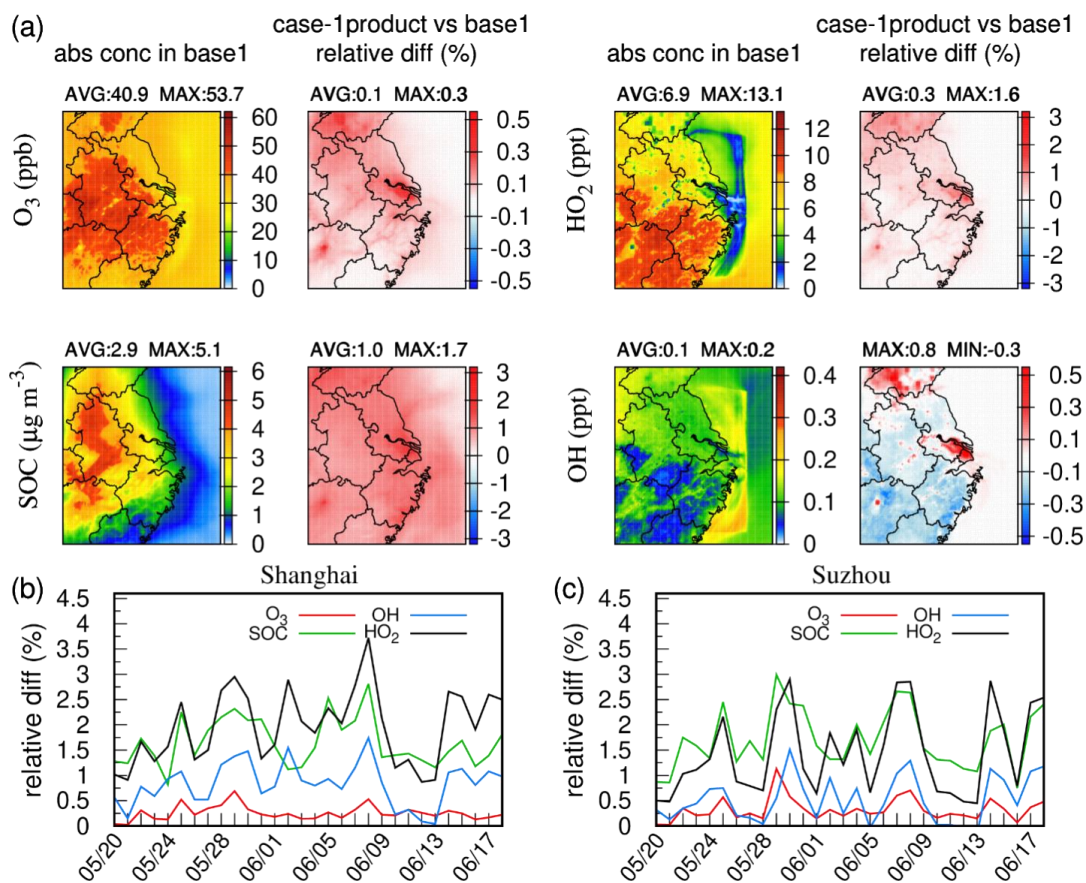
603

604 **Figure 2.** Diurnal variations of emissions (yellow line) and predicted concentrations (black line)
605 for 2-MN (a), 1-MN (c), and Nap (e), as well as the corresponding SOC concentrations (b, d, f) at
606 the Taizhou site.



607

608 **Figure 3.** Contributions of the major aromatic species to (a) the total emissions of aromatics and
 609 the aromatic-derived SOC in (b) case-1 product and (c) case-2 products at the Taizhou site. These
 610 aromatic species are Nap, 1-MN, 2-MN, BENZ, the sum of toluene and aromatics with $k_{OH} <$
 611 $2 \times 10^4 \text{ ppm}^{-1} \text{ min}^{-1}$ (ARO1+TOLU), and the sum of xylenes, 1,2,4-trimethyl benzene and aromatics
 612 with $k_{OH} > 2 \times 10^4 \text{ ppm}^{-1} \text{ min}^{-1}$ excluding Nap and MN (ARO2MN'+MPO+B124).



613

614 **Figure 4.** (a) Absolute concentrations of SOC, O₃, OH, and HO₂ in base1, and changes in case-

615 1product relative to base1, respectively. Daily relative changes in case-1product compared to

616 base1 at (b) Shanghai and (c) Suzhou.